Study of the corrosion resistance on nano-ZrO_2 doped MgO ceramic composites by copper slag.

L.V. García-Quiñonez
Centro de Investigación Científica y de Educación Superior de Ensenada Unidad Monterrey
L.F. Verdeja
Universidad de Oviedo
D. Fernández-González
Universidad de Oviedo
E. Castro-Soto
Universidad Autónoma de Nuevo León, Facultad de Ingeniería Mecánica y Eléctrica.
G.A. Castillo-Rodríguez
Universidad Autónoma de Nuevo León, Facultad de Ingeniería Mecánica y Eléctrica
E.A. Rodíguez-Castellanos
Universidad Autónoma de Nuevo León, Facultad de Ingeniería Mecánica y Eléctrica
A.M. Guzmán-Hernández
Universidad Autonoma de Nuevo Leon, Facultad de Ingeniería Mecánica y Eléctrica
C. Gómez-Rodríguez (cristiang1983@hotmail.com)
Universidad Autonoma de Nuevo Leon Facultad de Ingeniería Mecánica y Electríca
https://orcid.org/0000-0001-9124-6038

Rapid Communication

Keywords: Ceramic composites; corrosion; microstructure

Posted Date: August 17th, 2020

DOI: https://doi.org/10.21203/rs.3.rs-58174/v1

Abstract

This study investigated the corrosion mechanism on 100 wt. % MgO and 95 wt. % MgO with 5 wt. % nano-ZrO_2 ceramic composites. First, MgO powder and powder mixtures (MgO + nano ZrO_2) were uniaxially and isostatically pressed and, then, they were sintered at 1650 °C. Corrosion by copper slag was studied with sintered samples. Physical properties, microstructure and penetration of the slag in the refractory were studied. Results reveal that ZrO_2 nanoparticles enhanced the densification of the samples, promoting grain growth due to diffusion of vacancies during sintering process. Additionally, magnesia bricks were severely corroded, if compared with those doped with nano-ZrO_2, due to the dissolution of MgO grains during the chemical attack by copper slag.

1 Introduction

Copper metallurgy is mainly based on copper sulphides as chalcopyrite ($CuFeS_2$), bornite (Cu_5FeS_4) and chalcocite (Cu_2S) are the main ores. Thus, fusion-conversion process is the most widely used in the copper metallurgy to obtain the metal. The fusion process generates two immiscible phases: matte (mostly copper as sulphide) and slag (most of iron as fayalite). Copper in the slag will be as sulfide (matte) that was dragged or trapped by the slag, or as oxide associated to other oxides of the slag. Copper slags are disposed in dumps or sold as abrasives or gravel for mortar [1], when the copper content is < 2%. Likewise, matte and slag severely attack the refractory lining at a high temperature, being significative in the slag line of the furnaces, where bricks are mainly of: MgO-Cr_2O_3, MgO-Al_2O_3, MgO-CaO.

On the other hand, 35 Mt of copper are worldwide produced every year: 60% by pyrometallurgical processes and 40% from copper scrap [2]. Thus, copper industry is a great consumer of refractory materials as more than 25000 tons of refractory materials are used in its primary production (copper smelting, conversion and refining in furnaces) [2]. Therefore, the partial or total replacement of the refractory means a significant investment for copper companies. This way, researchers focus on obtaining refractory bricks with exceptional properties using nanotechnology [3, 4]. Within the exceptional properties, the resistance to the aggressive conditions of the immiscible phases involved in the copper production is included. This manuscript is aimed at studying the corrosion resistance of 100 wt. % MgO and 95 wt. % MgO with 5 wt. % nano-ZrO_2 ceramic composites by copper slag.

2 Materials And Methods

MgO with particle size < 45 μm and chemical composition (wt. %): SiO_2, 0.2; Al_2O_3, 0.15; Fe_20_3, 0.13; MgO, 98.5; CaO, 1; B_2O_3, 0.01; was used in the experiments. High purity nano-ZrO_2 was also used as raw material. A dispersion of acetone and anionic polymeric dispersant (Zephrym-PD3315) was used to prepare the green specimens. Samples were cold pressed to obtain the green specimen: first, uniaxially pressed (UP) in a steel mould at 100 MPa for 2 min and, then isostatically pressed (IP) at 200 MPa for

5 min. Finally, green specimens were sintered at 1650 °C for 4 hours. Physical properties were evaluated in terms of apparent porosity (AP) and bulk density (BD) by Archimedes method.

Copper slag was used to perform the corrosion test. The corrosion test consisted in determine the chemical resistance of the sintered refractory samples against the slag penetration. The corrosion experiments were done drilling a hole (~ 3.5 mm in diameter with 2.5 mm in depth) in the center of the upper face of the cylindrical sample and filling it with powder slag (5 g). The sintered samples analyzed in this chemical test were 25 mm in diameter and 6 mm in height. The experiment was carried out in an electric furnace at 1550 °C for 4 h at the maximum temperature. Both the heating and cooling rates were 5 °C/min. Afterward, samples were transversely cut using a diamond disc. After cutting, the surfaces of interest were polished with SiC paper for microscopy evaluation.

The cross-sections of polished sintered samples, before and after the chemical test were characterized by scanning electron microscope (SEM) (FEI-Model/Nova-NanoSEM200) with an energy disperse X-ray spectroscopy (EDX) detector, the measurements of the penetration distance were carried out through micrographs (SEM analysis) of the chemically attacked samples, likewise, Likewise, the slag concentration inside sample was detected through EDX microanalysis, detecting the variation in the chemical composition through the cross-sectional sample (from the base to the slag powder deposit).

Chemical composition of copper slag and MgO were determined by an X-ray fluorescence (XRF) spectrometer (Axios, PANalytical) with a Rh-anode X-ray tube with a maximum power of 4 kW. The presence of phases of copper slag and raw material were determined by X-ray diffraction (XRD) method, using a Bruker D8 Advance diffractometer operated at the tube voltage and current of 40 kV and of 30 mA respectively, with Cu-Ka radiation.

Table 1 collects the values of the chemical composition and phase percentage of the copper slag. Copper slag is mainly formed by fayalite (Fe_2SiO_4), magnetite (Fe_3O_4) and copper oxide and sulfide (0.5-2 wt. % Cu) as secondary phases. Iron is the main element in copper slags, > 40% [5, 6]. Data of XRF analysis collected in Table 1 indicate that the copper and iron contents (in wt.%) are 1.84 and 42.82, respectively, are in the above-mentioned ranges for copper slags

Table 1
Quantitative analysis of elements and phases percentages of the copper slag.

Copper slag			
Element/wt.%	**Element/wt.%**	**Element/wt.%**	**Element/wt.%**
Ca/1.756	Cr/0.02603	Al/3.239	Cu/1.84
O/36.15	Cl/0.02477	P/0.05097	Co/0.4598
Fe/42.82	K/0.6914	Ti/0.1994	Mo/0.1796
Si/10.36	Sr/0.01129	S/0.2197	As/0.1535
Mn/0.1327	Zn/0.2614	Na/0.993	Pb/0.1129
Phases percentages			
Fe_2SiO_4 = 85.80 ± 1.30 Fe_3O_4 = 7.90 ± 1.60 $CuFe_2O_4$ = 6.20 ± 1.80			

3 Results And Discussion

Figure 1. **(a)** XRD pattern of copper slag, **(b)** XRD pattern of samples with 95 wt. % MgO with 5 wt. % nano-ZrO_2 and 100 wt.% MgO, **(c-d)** SEM images of samples of 100 wt.% MgO and 95 wt. % MgO with 5 wt. % nano-ZrO_2, respectively.

Moreover, the above is related with the values obtained in BD for 100 wt.% MgO and 95 wt.% MgO with 5 wt. % of nano-ZrO_2, resulting 2.72 and 3.04 g/cm^2 for each one, as well as the AP values were 26. 25 and 14. 49%, respectively. In general, an increase in the density values was obtained with nanoadditions of ZrO_2. This behavior can be attributed to: an ionic migration, between the Zr that has a valence of + 4 and Mg has a valence of + 2, cationic magnesium vacancies in the cubic structure of MgO are generated due to the migration of magnesium ions when they replace zirconia ions. These cation vacancies at the border of the MgO grains have to be replaced by cations that come from crystalline structures internal to the volume of the MgO grain, in such a way that a cationic migration towards the grain border is carried out. This leads the grain border to begin to move, joining with each other with other grain boundaries. All this produces a contraction of the material, and the sample is densified.

3.1 100 wt. % MgO sample tested copper slag

Figure 2. **(a-c)** SEM images of samples with 100 wt.% MgO analysed with copper slag, **(d)** concentration of slag elements as a function of the penetration distance, **(e)** schematic representation where SEM (dots with letters) and EDX analyses (red line) were made.

3.2 95 wt. % MgO with 5 wt. % ZrO_2 sample tested copper slag

Figure 3 corresponds to the corrosion test of the sample with 95 wt. % MgO with 5 wt. % nano-ZrO_2 tested with copper slag. Figure 3**(a)** shows a micrograph corresponding to the upper-area of the sample (of the hole where the slag was deposited). Figure 3**(b)** shows the zone where the slag begins to infiltrate into the material. Likewise, in the Fig. 3**(b)**, the slag advances of two different manners: first, direct infiltration of slag particles that attacked the MgO grains (with a penetration depth of 25 μm from the hole, the grain is attacked), being this penetration depth less than in the 100 wt. % MgO sample; second, when the particles were inside the material, they dissolved in form of molten slag (liquid) through the grain boundaries (the slag circulates intergranularly). This kind of advancement of the slag was inhibited due to the ZrO_2 nanoparticles (phase of circular shape) since they act as barriers against the penetration of the intergranular liquid, observed as retention points (non-circular phase due to accumulation in different proportions of slag elements on the periphery of ZrO_2 nanoparticles) where the slag was retained around the ZrO_2 particles. Although the $CaZrO_3$ phase was not identified after chemical corrosion analysis, this phase also helped to hinder the penetration of the refractory and increased the viscosity of the low melting point phases of the molten slag, slowing down the intergranular path of the molten slag.

Figure 3. **(a-c)** SEM images of samples with 95 wt. % MgO with 5 wt. % nano-ZrO_2 analysed with copper slag, **(d)** concentration of slag elements depending on the penetration distance, **(e)** schematic representation where SEM (dots with letters) and EDX analyses (red line) were made.

4 Conclusion

The corrosion resistance of 100 wt. % MgO and 95 wt. % MgO with 5 wt. % nano-ZrO_2 ceramic composites by copper slag was studied in this manuscript. An increase in the bulk density of the samples with the addition of 5 wt.% of nano-ZrO_2 was evident, obtaining 3.04 g/cm^2. Also, it is observed that in the sample with 100 wt. % MgO, the penetration of the copper slag (3000 μm) is greater than in the sample of 95 wt. % MgO with 5 wt. % nano-ZrO_2 (~ 636 μm). In this last ones, ZrO_2 nanoparticles acted as retention points to stop intergranular infiltration of the copper slag blocking its path.

References

[1] Sancho JP, Verdeja LF, Ballester A. *Metalurgia Extractiva Volumen II. Procesos de Obtención*. Madrid (ES): Sintesis Madrid, 2000.

[2] Fisher RE. Refractory usage in nonferrosos metallurgical applications. In *3r^d Unified International Conference on Refractories.* Krietz L, Leung JG, Eds. Brazil: Unitecr, 1993: 131-142.

[3] Gómez-Rodríguez C, Fernández-González D, García-Quiñonez LV, et al. MgO refractory doped with ZrO_2 nanoparticles: influence of cold isostatic and uniaxial pressing and sintering temperature in the physical and chemical properties. *Metals* 2019, **9**: 1-20.

[4] Ghasemi-Kahrizsangi S, Dehsheikh HG, Karamian E. Impact of Titania nanoparticles addition on the microstructure and properties of MgO-C refractories. *Ceram Int* 2017, **43**: 15472-15477.

[5] Coursol P, Cardona N, Valencia, et al. Minimization of Copper Losses in Copper Smelting Slag During Electric Furnace Treatment. *JOM* 2012, **64**: 1305-1313.

[6] Shi C, Meyer C, Behnood A. Utilization of copper slag in cement and concrete. *Resour Conserv Recy* 2008, **52**: 1115-1120.

[7] Verdeja LF, Sancho JP. *Refractory and ceramic materials*. Madrid (ES): Sintesis Madrid, 2008.

Figures

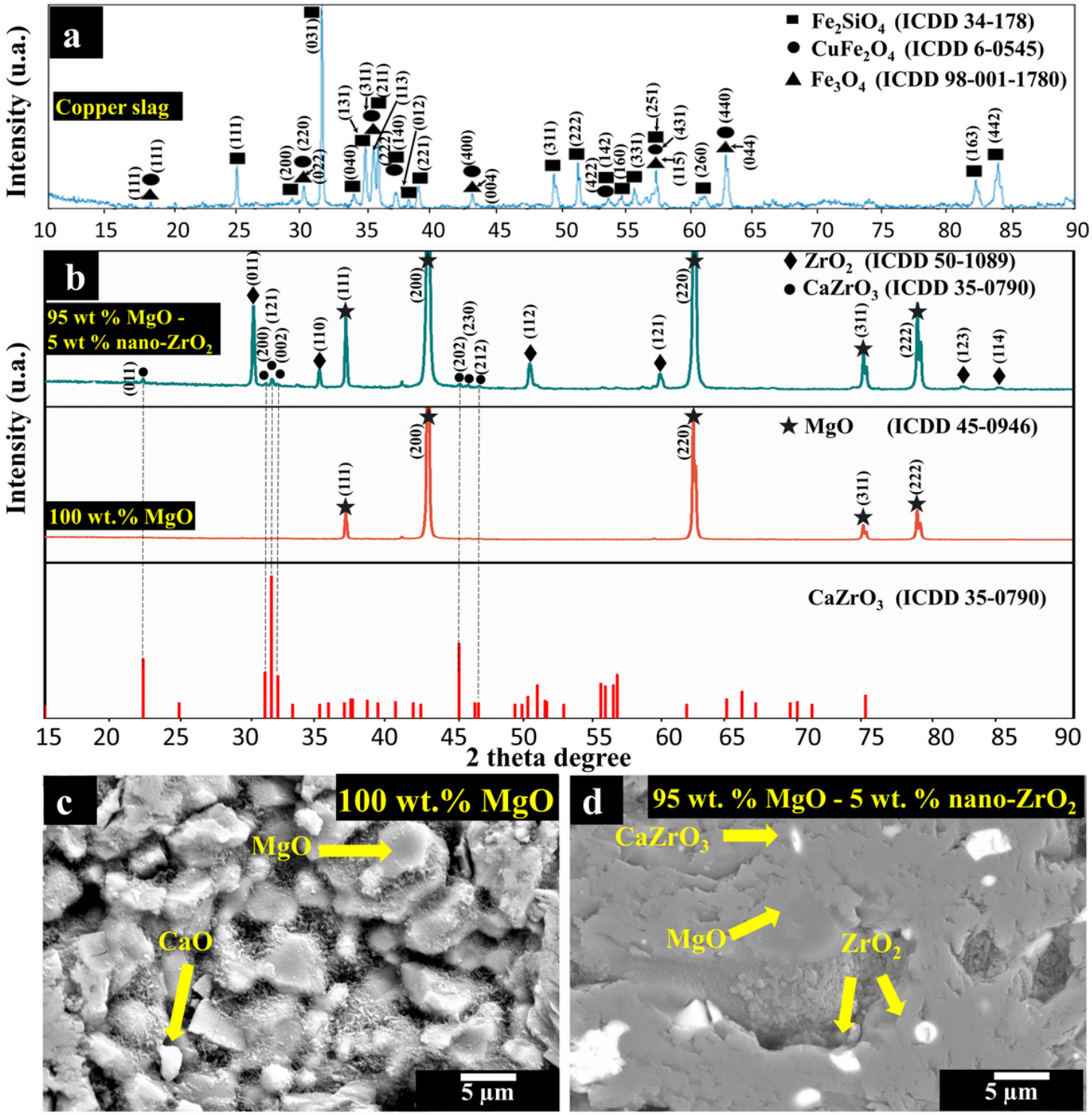

Figure 1

(a) XRD pattern of copper slag, (b) XRD pattern of samples with 95 wt. % MgO with 5 wt. % nano-ZrO2 and 100 wt.% MgO, (c-d) SEM images of samples of 100 wt.% MgO and 95 wt. % MgO with 5 wt. % nano-ZrO2, respectively.

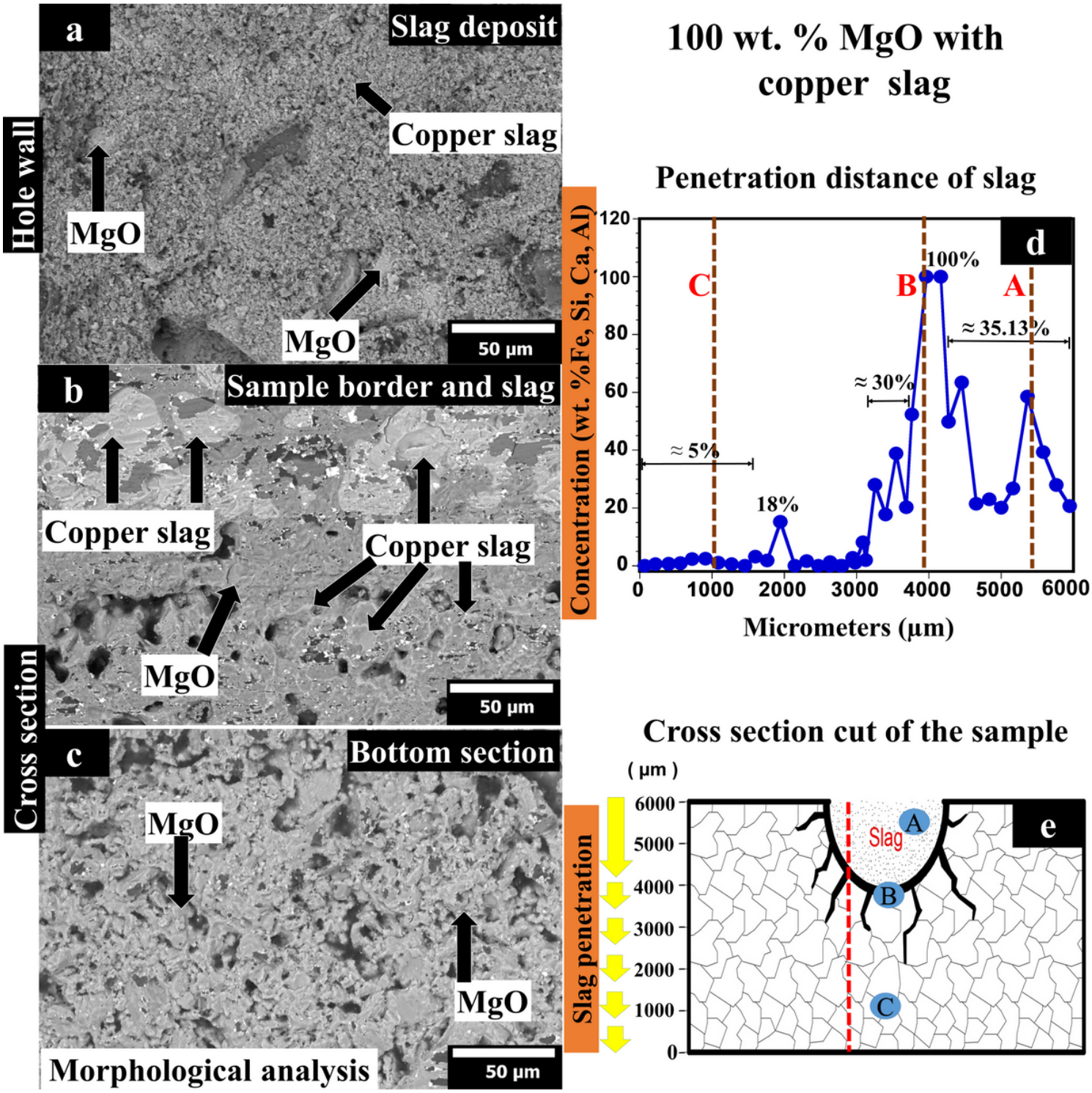

Figure 2

(a-c) SEM images of samples with 100 wt.% MgO analysed with copper slag, (d) concentration of slag elements as a function of the penetration distance, (e) schematic representation where SEM (dots with letters) and EDX analyses (red line) were made.

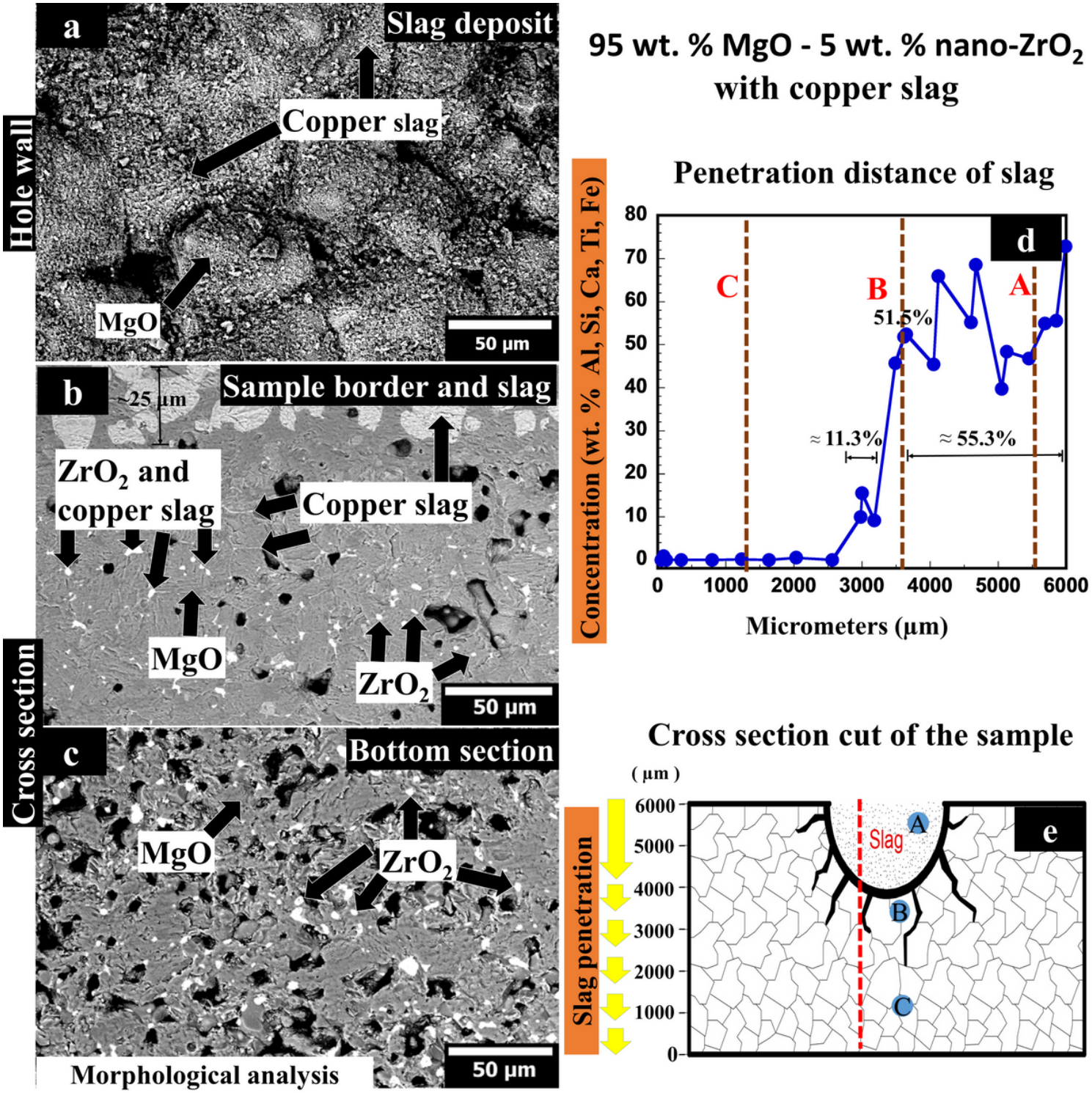

Figure 3

(a-c) SEM images of samples with 95 wt. % MgO with 5 wt. % nano-ZrO2 analysed with copper slag, (d) concentration of slag elements depending on the penetration distance, (e) schematic representation where SEM (dots with letters) and EDX analyses (red line) were made.